

Molecular gas mass functions of normal star forming galaxies since $z \sim 3$ [★]

S. Berta¹, D. Lutz¹, R. Nordon², R. Genzel¹, B. Magnelli³, P. Popesso¹, D. Rosario¹, A. Saintonge¹, S. Wuyts¹, and L. J. Tacconi¹

¹ Max-Planck-Institut für extraterrestrische Physik (MPE), Postfach 1312, 85741 Garching, Germany.

² School of Physics and Astronomy, The Raymond and Beverly Sackler Faculty of Exact Sciences, Tel-Aviv University, Tel-Aviv 69978, Israel.

³ Argelander-Institut für Astronomie, Universität Bonn, Auf dem Hügel 71, D-53121 Bonn, Germany

Received ...; accepted ...

ABSTRACT

We use deep far-infrared data from the PEP/GOODS-*Herschel* surveys and rest frame ultraviolet photometry to study the evolution of the molecular gas mass function of normal star forming galaxies. Computing the molecular gas mass, M_{mol} , by scaling star formation rates (SFR) through depletion timescales, or combining IR luminosity and obscuration properties as in Nordon et al., we obtain M_{mol} for roughly 700, $z = 0.2 - 3.0$ galaxies near the star forming “main sequence”. The number density of galaxies follows a Schechter function of M_{mol} . The characteristic mass M^* is found to strongly evolve up to $z \sim 1$, and then to flatten at earlier epochs, resembling the infrared luminosity evolution of similar objects. At $z \sim 1$, our result is supported by an estimate based on the stellar mass function of star forming galaxies and gas fraction scalings from the PHIBSS survey. We compare our measurements to results from current models, finding better agreement with those that are treating star formation laws directly rather than in post-processing. Integrating the mass function, we study the evolution of the M_{mol} density and its density parameter Ω_{mol} .

Key words. Galaxies: mass function – Galaxies: statistics – Galaxies: evolution – Galaxies: star formation – Infrared: galaxies

1. Introduction

Stars form in cold, dense molecular clouds, and the molecular gas content of galaxies is an important constraint to galaxy evolution. In the interplay between accretion of gas, star formation, metal enrichment, and outflows, the molecular gas content reflects the prevailing physical processes (e.g. Bouché et al. 2010; Davé et al. 2010; Lilly et al. 2013). For the cosmic baryon budget (e.g. Fukugita et al. 1998), molecular gas can be of increasing relative importance at high redshifts where galaxies are gas-rich.

Molecular gas is generally quantified using the CO molecule as a tracer. Local samples include several hundred targets (e.g. Saintonge et al. 2011, and references therein), but CO detections of star-forming, intermediate/high redshift galaxies are still limited to modest statistics of mostly very luminous galaxies (Carilli & Walter 2013, and references therein). For normal star forming galaxies, the PHIBSS survey (Tacconi et al. 2013) derives scaling relations on the basis of CO detections of 52 normal star forming galaxies at $z \sim 1.2$ and $z \sim 2.2$. In galaxies near the star-forming “main sequence” (MS, e.g. Noeske et al. 2007; Elbaz et al. 2007; Daddi et al. 2007), the molecular gas mass, M_{mol} , scales as SFR through a depletion time scale τ_{dep} that is only very slowly dependent on redshift (Tacconi et al. 2013).

Keres et al. (2003) reported the first attempt to derive the local molecular gas mass function, based on a sample of IRAS selected objects. To date, no derivation of a $z > 0$ mass function

has been possible, due to the heterogeneity and paucity of the available detections.

These difficulties have sparked interest in methods using dust mass as a tool to derive masses of the cold ISM of (distant) galaxies (e.g. Magdis et al. 2011, 2012; Scoville 2012). Dust mass is converted into gas mass by adopting a metallicity, and a scaling of gas-to-dust ratio with metallicity. Typically, to derive dust masses, these methods require photometry on the restframe-submm tail of the SED, or accurate multi-band data closer to the rest far-infrared (FIR) SED peak. Such requirements are still not met individually for large samples of normal high- z galaxies (Berta et al. in prep.). In a study of the restframe ultraviolet (UV) and FIR properties of *Herschel* galaxies, Nordon et al. (2013) established a method to derive M_{mol} of MS galaxies on the basis of their rest-FIR luminosity and rest-UV obscuration: properties which are readily available for larger samples. Here we apply the τ_{dep} scaling and the Nordon et al. recipe to the deepest *Herschel* (Pilbratt et al. 2010) FIR extragalactic observations and related restframe UV data to derive M_{mol} of MS galaxies, which are known to power $\sim 90\%$ of the cosmic star formation (Rodighiero et al. 2011). On this basis, we construct their molecular gas mass function and study its evolution since $z \sim 3$.

We adopt a Λ CDM cosmology with $(h, \Omega_m, \Omega_\Lambda) = (0.70, 0.27, 0.73)$ and a Chabrier (2003) initial mass function.

2. Derivation of molecular gas mass and source selection

We use the deepest PACS (Poglitsch et al. 2010) far-infrared survey, combining the PACS Evolutionary Probe (PEP, Lutz et al. 2011) and GOODS-*Herschel* (Elbaz et al. 2011) data in the

Send offprint requests to: Stefano Berta, e-mail: berta@mpe.mpg.de

[★] *Herschel* is an ESA space observatory with science instruments provided by European-led Principal Investigator consortia and with important participation from NASA.

GOODS-N and GOODS-S fields. We defer to Magnelli et al. (2013) for details about data reduction and catalog extraction.

Ancillary data come from the catalogs built by Berta et al. (2011) and Grazian et al. (2006, MUSIC), both including photometry from the U to *Spitzer* IRAC bands. To these we add *Spitzer* MIPS 24 μm (Magnelli et al. 2011), IRS 16 μm data (Teplitz et al. 2011), GALEX DR6 data, and a collection of optical spectroscopic redshifts (see Berta et al. 2011, for details). When needed, photometric redshifts are used, reaching accuracies of $\Delta(z)/(1+z)=0.04$ and 0.06 in the two fields, respectively (Berta et al. 2011; Santini et al. 2009).

Based on current CO observations of local and $z \sim 1$ objects (e.g. Saintonge et al. 2011, 2012; Tacconi et al. 2013), the relation between M_{mol} and SFR of MS galaxies can be described as a simple scaling with a depletion time scale mildly dependent on redshift: $M_{\text{mol}}/\text{SFR} = \tau_{\text{dep}}$, with $\tau_{\text{dep}} = 1.5 \cdot 10^9 \times (1+z)^{-1}$ [Gyr]. Second order effects, likely driven by the actual distribution of dust and gas in galaxies, have been studied by Nordon et al. (2013), while investigating the infrared excess (IRX) and the observed UV slope β of $1.0 < z < 2.5$ PEP galaxies (Meurer et al. 1999). Using a smaller sample of $z \geq 1$ galaxies with CO gas masses, Nordon et al. study the link between A_{IRX} and molecular gas content, finding a tight relation between the scatter in the $A_{\text{IRX}}-\beta$ plane and the specific attenuation contributed by the molecular gas mass per young star. Here¹ $A_{\text{IRX}} = 2.5 \log(\text{SFR}_{\text{IR}}/\text{SFR}_{\text{UV}} + 1)$ represents the effective UV attenuation. These authors derive the equation

$$\log\left(\frac{M_{\text{mol}}}{[10^9 M_{\odot}]}\right) = \log\left(\frac{A_{\text{IRX}} \cdot \text{SFR}}{[M_{\odot} \text{yr}^{-1}]}\right) - 0.20(A_{\text{IRX}} - 1.26\beta) + 0.09, (1)$$

where the SFR includes both IR and UV contributions. This provides an estimate of molecular gas mass (already including the contribution of Helium) using only widely available integrated rest-frame UV and FIR photometry, consistent with $z \sim 1$ depletion times by calibration. We use the FIR and UV photometry to apply the Tacconi et al. (2013) τ_{dep} scaling and the Nordon et al. (2013) recipe to ~ 700 MS galaxies in our survey. We stress again that both methods rely on calibrations based on CO observations and are thus valid under the assumption that the adopted values of the CO-to-molecular gas mass conversion factor, α_{CO} , are correct (see Tacconi et al. 2013; Nordon et al. 2013).

$\text{SFR}_{\text{IR,UV}}$ are computed using the Kennicutt (1998) calibrations. Infrared luminosities, $L(\text{IR})$, are derived by SED fitting with the Berta et al. (2013) templates library. Alternative methods (e.g. Wuyts et al. 2011; Nordon et al. 2012) lead to equivalent results within a 10-20% scatter (see Berta et al. 2013). UV parameters are derived from the restframe 1600 and 2800 \AA luminosities, following the procedure of Nordon et al. (2013).

Uncertainties on M_{mol} are computed combining the systematic errors embedded in the adopted equations and statistical uncertainties due to the scatter on observed quantities. Tacconi et al. (2013) estimate a systematic uncertainty of 50% in their M_{mol} , which is thus reflected into the our τ_{dep} -based estimate. Nordon et al. (2013) evaluate that the accuracy of Eq. 1 is 0.12 dex for their collection of $z \geq 1$ MS galaxies and 0.16 dex when validating on $z \sim 0$ MS galaxies from Saintonge et al. (2011, 2012). We performed 10000 Monte Carlo realizations of M_{mol} for each galaxy assuming Gaussian distributions for the mentioned sources of errors and accounting also for the contribution of the template library intrinsic scatter to the $L(\text{IR})$ uncertainty. As a result, the median uncertainty on M_{mol} obtained

¹ SFR_{IR} is based on bolometric IR luminosity; SFR_{UV} is derived from UV continuum, uncorrected for dust attenuation.

through Eq. 1 is $\sim 40\%$, without accounting for Tacconi et al. (2013) systematics, and is larger than 50% for only $\sim 10\%$ of the sample.

Sample selection is driven by the need to compute total SFRs and by the requirements imposed by Eq. 1. We limit the analysis to galaxies lying within $|\Delta \log(\text{SFR})_{\text{MS}}| \leq 0.5$ from the MS. The MS is assumed to have unit slope in the stellar mass vs. star formation rate (M_{\star} -SFR) plane, and a specific-SFR normalization varying as $\text{sSFR}_{\text{MS}}[\text{Gyr}^{-1}] = 26 \times t_{\text{cosmic}}^{-2.2}$ (Elbaz et al. 2011).

We apply a 3σ flux cut at 160 μm , the band that best correlates with $L(\text{IR})$ (Elbaz et al. 2011; Nordon et al. 2012). When deriving UV parameters, it is important to avoid contamination of observed bands by the 2100 \AA carbonaceous absorption feature. Combining GALEX and optical photometry, we define four redshift windows: $0.2 < z \leq 0.6$, $0.7 < z \leq 1.0$, $1.0 < z \leq 2.0$, and $2.0 < z \leq 3.0$. This choice reduces the loss of sources due to restframe UV requirements to $< 2\%$. The total number of sources in each redshift bin is included in Table 1. Our sample contains 43 galaxies hosting an X-ray AGN, of which only 4 are Type-1. Distributions of $L(\text{IR})$ and β for the AGN galaxies are similar to those of inactive ones. We have verified that our conclusions below are not affected by the inclusion of these AGN hosts.

3. The molecular gas mass function

The comoving number density of galaxies in intervals of M_{mol} is computed adopting the well known $1/V_a$ formalism:

$$\Phi(M) \Delta M = \sum_i \frac{1}{V_a^i} \Delta M \quad (2)$$

where the sum is computed over all sources in the given M_{mol} bin. The accessible volume V_a is a spherical shell delimited by $z_{\text{min}}^{\text{bin}}$ and $\min(z_{\text{max}}, z_{\text{max}}^{\text{bin}})$. Here z_{max} is the maximum redshift at which a galaxy would be observable in our survey (Schmidt 1968), and $z_{\text{min,max}}^{\text{bin}}$ define redshift bins.

Source selection is mainly based on a 160 μm cut, and the UV requirements do not produce significant source losses. On the other hand, the conversion from $S(160)$ to $L(\text{IR})$ is obtained adopting a family of SED templates spanning a variety of colors. Moreover UV properties are also involved in computing total SFR and in applying Eq. 1.

As a consequence, the conversion between 160 μm fluxes and molecular gas mass is not unique, but comprises a distribution of “mass to light ratios”. Because of this scatter in M_{mol} vs. $S(160)$, a flux cut induces a molecular mass incompleteness. This effect was thoroughly studied by Fontana et al. (2004) and Berta et al. (2007), among others, in the case of stellar mass. Equivalently, the recipe defined by these authors can be applied to the specific case of molecular gas mass and FIR fluxes to derive completeness corrections as a function of M_{mol} . Using the distribution of the parent MS population, and comparing it to that of PACS galaxies leads to similar results.

The comoving number density of galaxies is shown in Fig. 1. Results from the τ_{dep} scaling or Eq. 1 are very similar, thus only the latter are shown. Table 1 reports both estimates, along with average completeness values for each mass bin, which also includes the photometric completeness of the FIR catalogs.

An independent characterization of the mass function is provided by the maximum likelihood approach by Sandage, Tammann & Yahil (1979, STY). We adopt the Bayesian implementation by Berta et al. (2007) and adapt it to our case, thus

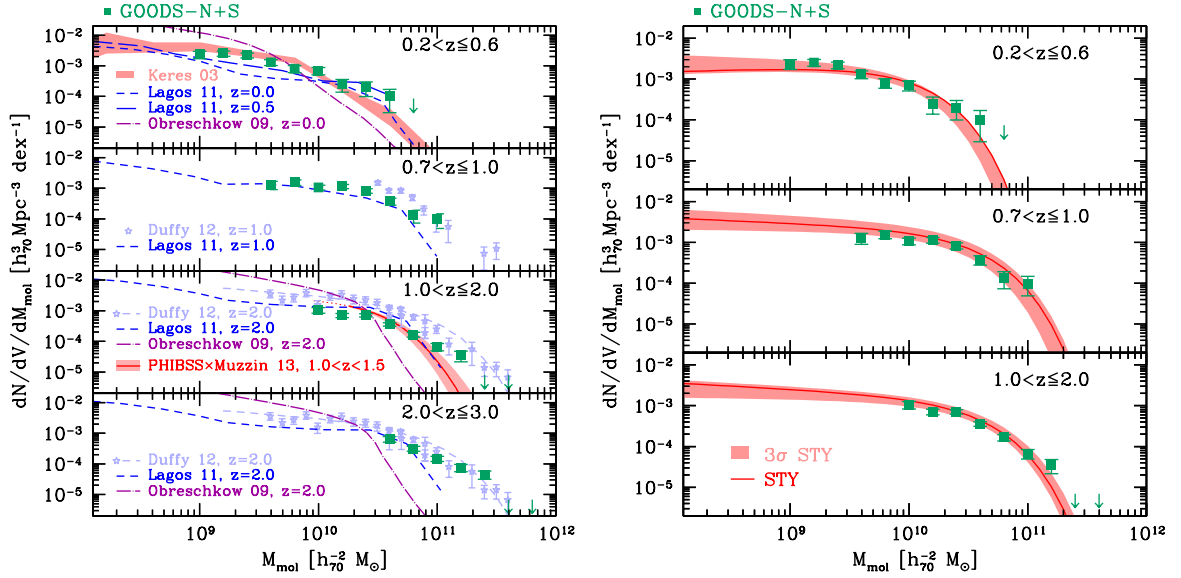


Fig. 1. The molecular gas mass function of *Herschel* galaxies. *Left:* comparison of the $1/V_a$ estimate (green squares, based on Eq. 1) to literature data (Keres et al. 2003) and models (Obreschkow & Rawlings 2009a; Lagos et al. 2011; Duffy et al. 2012). The red line and shaded area at $z = 1.0 - 2.0$ are obtained scaling the Muzzin et al. (2013) stellar mass function using the molecular gas fractions by Tacconi et al. (2013). When needed, masses found in the literature were scaled by the factor 1.36 necessary to account for Helium, and matched to our set of cosmological parameters. *Right:* results of the parametric STY evaluation of a Schechter mass function (red lines) and its 3σ uncertainty (shaded areas).

fully propagating the actual M_{mol} uncertainties into the parametric function evaluation. The adopted functional form to describe the mass function is a Schechter (1976) function:

$$\Phi(M)dM = \frac{\Phi^*}{M^*} \left(\frac{M}{M^*} \right)^\alpha e^{-\frac{M}{M^*}} dM, \quad (3)$$

where Φ^* represents the normalization, α the slope in the low mass regime, and M^* the transition mass between a power-law and the exponential drop-off and the e-folding mass of the latter. Berta et al. (2007) provide more details about this method. Table 2 includes the most probable parameter values and their 3σ uncertainties, obtained with both M_{mol} estimates. The right-hand panel of Fig. 1 compares the result of the STY analysis to the $1/V_a$ mass function. No STY analysis is attempted for the highest redshift bin, because only the very massive end is covered.

The Schechter M^* parameter increases by more than a factor of 3 between $z = 0.4$ and 0.8 , and then flattens at $z > 1$. This rate resembles the evolution of the IR luminosity function of normal star forming galaxies (Gruppioni et al. 2013), and reflects the link between SFR and M_{mol} . At the same time, Φ^* varies by only a factor of 2 over the $0.4-1.5$ redshift range. The net effect is a significant evolution of the number density of galaxies with large M_{mol} , while at the low mass end it remains roughly constant. Finally, the most probable value of α steepens as redshift increases, but this might be simply an effect of the different mass ranges effectively constrained at different redshifts (note that the 3σ confidence levels are consistent with nearly no evolution).

We compare this M_{mol} mass function to an estimate based on stellar mass. Using the PHIBSS CO survey, Tacconi et al. (2013, see their Fig. 12) compute molecular gas fractions for $z = 1.0 - 1.5$ normal star forming galaxies, as a function of M_* . We combine these gas fractions with the $z = 1.0-1.5$ stellar mass function of star forming galaxies by Muzzin et al. (2013, see also Ilbert et al. 2013; Drory et al. 2009). To account for the MS width in this estimate, we apply a 0.2 dex Gaussian smoothing. The result is close to the observed mass function at $z = 1.0 - 2.0$ (Fig.

1). Note also the related approach of Sargent et al. (in prep.), as quoted in Carilli & Walter (2013).

4. Discussion

Our observed M_{mol} function is computed only for normal star forming galaxies within ± 0.5 dex in SFR from the main sequence. Thus it represents a lower limit to the total M_{mol} mass function, by missing passive (low SFR) galaxies and powerful, above-sequence objects. Passive galaxies will provide a negligible contribution unless they include a hypothetical population of molecular gas-rich galaxies forming stars with very low efficiency. For reference, local passive galaxies, lying at $\Delta(\text{sSFR})_{\text{MS}} \leq -1.0$ dex, have molecular gas fractions $f_{\text{mol}} \leq 2\%$ (Saintonge et al. 2012). Also star bursting galaxies, i.e. those lying above the MS, should play only a minor role in shaping the mass function. Rodighiero et al. (2011) have shown that the contribution of above-sequence sources to the number density of star forming galaxies and total star formation rate density at $z = 1.5 - 2.5$ is small. For our $\Delta \log(\text{SFR})_{\text{MS}} = 0.5$ cut, we find that objects above the MS contribute no more than $\sim 4\%$ to the number density of star forming galaxies, and $\sim 16\%$ to their SFR density. Depending on whether galaxies rise above the main sequence mostly due to an increased star formation efficiency at fixed gas mass, or due to larger gas masses, the effect on the mass function will vary between a global upward $\sim 4\%$ shift or a preferential increase at higher gas masses within the limits permitted by the 16% SFR contribution. Saintonge et al. (2012) show that in local starbursts the two effects share a 50%-50% role in causing SFR changes with respect to the MS.

Our results are compared in Fig. 1 to the Keres et al. (2003) local CO mass function of IRAS-selected galaxies. Applying a variable CO-to- H_2 conversion factor, inversely dependent on $L(\text{CO})$ itself, Obreschkow & Rawlings (2009b,a) obtained a revisited mass function quickly dropping at the high-

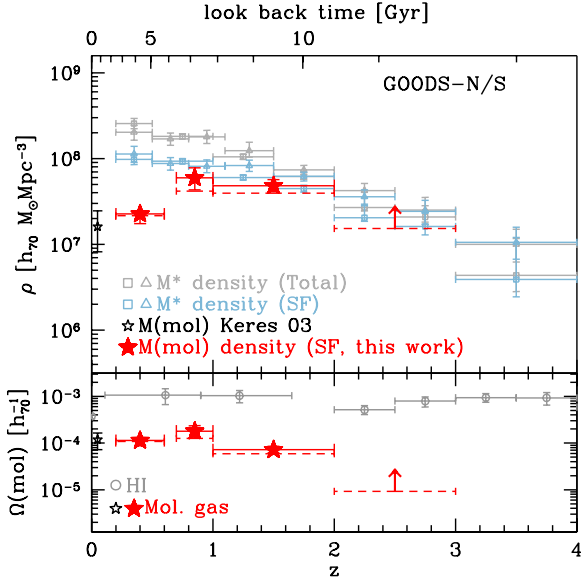


Fig. 2. *Top:* redshift evolution of the molecular gas mass density, based on Eq. 1. Red symbols and solid error bars belong to the total mass density; dashed error bars mark lower limits limited to the mass range covered by observations. The black star is computed by integrating the local mass function (Keres et al. 2003). Grey squares and triangles represent the total M_* density by Ilbert et al. (2013) and Muzzin et al. (2013), respectively. Light blue symbols belong to star forming galaxies only. *Bottom:* evolution of Ω_{mol} (red symbols, this work) and Ω_{HI} (Prochaska & Herbert-Fort 2004; Zwaan et al. 2005; Rao et al. 2006), where we have divided the latter by 1.3 in order to avoid counting Helium twice.

mass end. Modeling was implemented by post-processing the De Lucia & Blaizot (2007) semi analytic (SAM) results, and assigning the atomic and molecular gas content to galaxies via a set of physical prescriptions (see Obreschkow et al. 2009). Their expectations (Fig. 1) tend to predict a too steep mass function both at low and high redshift. A second model based on the SAM approach was developed by Lagos et al. (2011), starting from the Bower et al. (2006) galaxy formation model. As in the case of Obreschkow & Rawlings (2009a) the Blitz & Rosolowsky (2006) star formation law is adopted, but in this case it is implemented throughout the galaxy evolution process in the SAM model. The model was tested against the observed stellar mass density evolution and the atomic and molecular gas content of local galaxies. Results are shown in Fig. 1, and are now much closer to our observed mass function up to $z \sim 2$. Figure 1 finally includes predictions of the hydrodynamical simulation by Duffy et al. (2012), which overall tend to overestimate the mass function, but are consistent with data at the observed high-mass tail.

Adopting the STY Schechter results, we integrate the mass function from $10^7 M_\odot$ to infinity and obtain a measure of the molecular gas mass density (see Table 2 and top panel of Fig. 2). A second estimate obtained by limiting the integral to the mass range effectively covered by observations is also provided. The molecular gas mass density increases by a factor of ~ 4 from $z = 0$ to $z = 1$ and then remains almost constant up to $z \sim 2$. For reference we plot also the M_* density (Muzzin et al. 2013; Ilbert et al. 2013) up to $z = 4$. The different trends re-

flect the growth of gas fractions as a function of redshift (e.g., Tacconi et al. 2013).

Finally, we compute the redshift evolution of the density parameter $\Omega_{\text{mol}}(z) = \rho_{\text{mol}}(z)/\rho_c(z)$ (Fig. 2 and Table 2), where the critical density at the given redshift is given by $\rho_c(z) = \frac{3H^2(z)}{8\pi G}$. The molecular gas density parameter peaks at $z \sim 1.0$; for comparison Ω_{HI} , derived from damped Ly- α systems (Prochaska & Herbert-Fort 2004; Rao et al. 2006), and including also low column density cases, does not evolve between $z=0.5$ and 4.0.

Using the deepest *Herschel* extragalactic observations available and restframe UV information for roughly 700 main sequence galaxies, we have built the first molecular gas mass function at redshift $z > 0$, and the first estimate of its density evolution up to $z = 3$. While future mm/submm surveys will significantly improve our knowledge of the molecular content in high- z galaxies, we have provided a basis for refinement of galaxy evolution models that are accounting for the molecular phase.

Acknowledgements. PACS has been developed by a consortium of institutes led by MPE (Germany) and including UVIE (Austria); KU Leuven, CSL, IMEC (Belgium); CEA, LAM (France); MPIA (Germany); INAF-IFSI/OAA/OAP/OAT, LENS, SISSA (Italy); IAC (Spain). This development has been supported by the funding agencies BMVIT (Austria), ESA-PRODEX (Belgium), CEA/CNES (France), DLR (Germany), ASI/INAF (Italy), and CICYT/MCYT (Spain).

References

- Berta, S., Lonsdale, C. J., Polletta, M., et al. 2007, *A&A*, 476, 151
 Berta, S., Lutz, D., Santini, P., et al. 2013, *A&A*, 551, A100
 Berta, S., Magnelli, B., Nordon, R., et al. 2011, *A&A*, 532, A49
 Blitz, L. & Rosolowsky, E. 2006, *ApJ*, 650, 933
 Bouché, N., Dekel, A., Genzel, R., et al. 2010, *ApJ*, 718, 1001
 Bower, R. G., Benson, A. J., Malbon, R., et al. 2006, *MNRAS*, 370, 645
 Carilli, C. & Walter, F. 2013, *ArXiv:1301.0371*
 Chabrier, G. 2003, *PASP*, 115, 763
 Daddi, E., Dickinson, M., Morrison, G., et al. 2007, *ApJ*, 670, 156
 Davé, R., Finlator, K., Oppenheimer, B. D., et al. 2010, *MNRAS*, 404, 1355
 De Lucia, G. & Blaizot, J. 2007, *MNRAS*, 375, 2
 Drory, N., Bundy, K., Leauthaud, A., et al. 2009, *ApJ*, 707, 1595
 Duffy, A. R., Kay, S. T., Battye, R. A., et al. 2012, *MNRAS*, 420, 2799
 Elbaz, D., Daddi, E., Le Borgne, D., et al. 2007, *A&A*, 468, 33
 Elbaz, D., Dickinson, M., Hwang, H. S., et al. 2011, *A&A*, 533, A119
 Fontana, A., Pozzetti, L., Donnarumma, I., et al. 2004, *A&A*, 424, 23
 Fukugita, M., Hogan, C. J., & Peebles, P. J. E. 1998, *ApJ*, 503, 518
 Grazian, A., Fontana, A., de Santis, C., et al. 2006, *A&A*, 449, 951
 Gruppioni, C., Pozzi, F., Rodighiero, G., et al. 2013, *ArXiv:1302.5209*
 Ilbert, O., McCracken, H. J., Le Fevre, O., et al. 2013, *ArXiv:1301.3157*
 Kennicutt, Jr., R. C. 1998, *ARA&A*, 36, 189
 Keres, D., Yun, M. S., & Young, J. S. 2003, *ApJ*, 582, 659
 Lagos, C. D. P., Baugh, C. M., Lacey, C. G., et al. 2011, *MNRAS*, 418, 1649
 Lilly, S. J., Carollo, C. M., Pipino, A., Renzini, A., & Peng, Y. 2013, *ArXiv:1303.5059*
 Lutz, D., Poglitsch, A., Altieri, B., et al. 2011, *A&A*, 532, A90
 Magdis, G. E., Daddi, E., Béthermin, M., et al. 2012, *ApJ*, 760, 6
 Magdis, G. E., Daddi, E., Elbaz, D., et al. 2011, *ApJ*, 740, L15
 Magnelli, B., Elbaz, D., Chary, R. R., et al. 2011, *A&A*, 528, A35
 Magnelli, B., Popesso, P., Berta, S., et al. 2013, *ArXiv:1303.4436*
 Meurer, G. R., Heckman, T. M., & Calzetti, D. 1999, *ApJ*, 521, 64
 Muzzin, A., Marchesini, D., Stefanon, M., et al. 2013, *ArXiv:1303.4410*
 Noeske, K. G., Weiner, B. J., Faber, S. M., et al. 2007, *ApJ*, 660, L43
 Nordon, R., Lutz, D., Genzel, R., et al. 2012, *ApJ*, 745, 182
 Nordon, R., Lutz, D., Saintonge, A., et al. 2013, *ApJ*, 762, 125
 Obreschkow, D., Croton, D., De Lucia, G., Khochfar, S., & Rawlings, S. 2009, *ApJ*, 698, 1467
 Obreschkow, D. & Rawlings, S. 2009a, *ApJ*, 696, L129
 Obreschkow, D. & Rawlings, S. 2009b, *MNRAS*, 394, 1857
 Pilbratt, G. L., Riedinger, J. R., Passvogel, T., et al. 2010, *A&A*, 518, L1
 Poglitsch, A., Waelkens, C., Geis, N., et al. 2010, *A&A*, 518, L2
 Prochaska, J. X. & Herbert-Fort, S. 2004, *PASP*, 116, 622
 Rao, S. M., Turnshek, D. A., & Nestor, D. B. 2006, *ApJ*, 636, 610
 Rodighiero, G., Daddi, E., Baronchelli, I., et al. 2011, *ApJ*, 739, L40

- Saintonge, A., Kauffmann, G., Kramer, C., et al. 2011, MNRAS, 415, 32
Saintonge, A., Tacconi, L. J., Fabello, S., et al. 2012, ApJ, 758, 73
Sandage, A., Tammann, G. A., & Yahil, A. 1979, ApJ, 232, 352
Santini, P., Fontana, A., Grazian, A., et al. 2009, A&A, 504, 751
Schechter, P. 1976, ApJ, 203, 297
Schmidt, M. 1968, ApJ, 151, 393
Scoville, N. Z. 2012, ArXiv:1210.6990
Tacconi, L. J., Neri, R., Genzel, R., et al. 2013, in press, see ApJ, 768, 64,
ArXiv:1211.5743
Teplitz, H. I., Chary, R., Elbaz, D., et al. 2011, AJ, 141, 1
Wuyts, S., Förster Schreiber, N. M., Lutz, D., et al. 2011, ApJ, 738, 106
Zwaan, M. A., Meyer, M. J., Staveley-Smith, L., & Webster, R. L. 2005,
MNRAS, 359, L30

Table 1. The molecular gas mass function of *Herschel* galaxies, derived with the $1/V_a$ method.

$\log(M_{\text{mol}})$ [$h_{70}^{-2} M_{\odot}$]	$0.2 < z \leq 0.6$			$0.7 < z \leq 1.0$			$1.0 < z \leq 2.0$			$2.0 < z \leq 3.0$		
	$\Phi(M)$ Eq. 1	$\Phi(M)$ τ_{dep}	Compl.	$\Phi(M)$ Eq. 1	$\Phi(M)$ τ_{dep}	Compl.	$\Phi(M)$ Eq. 1	$\Phi(M)$ τ_{dep}	Compl.	$\Phi(M)$ Eq. 1	$\Phi(M)$ τ_{dep}	Compl.
	[$10^{-4} h_{70}^3 \text{Mpc}^{-3} \text{dex}^{-1}$]			[$10^{-4} h_{70}^3 \text{Mpc}^{-3} \text{dex}^{-1}$]			[$10^{-4} h_{70}^3 \text{Mpc}^{-3} \text{dex}^{-1}$]			[$10^{-4} h_{70}^3 \text{Mpc}^{-3} \text{dex}^{-1}$]		
9.0	23.42±6.26	–	0.52	–	–	–	–	–	–	–	–	–
9.2	25.38±4.80	18.42±5.11	0.67	–	–	–	–	–	–	–	–	–
9.4	22.01±4.02	24.42±4.39	0.78	–	–	–	–	–	–	–	–	–
9.6	13.00±2.77	17.86±3.32	0.86	12.84±3.87	20.15±6.08	0.61	–	–	–	–	–	–
9.8	8.06±2.08	16.85±2.98	0.98	15.54±3.24	11.50±2.64	0.75	–	–	–	–	–	–
10.0	6.97±1.86	10.46±2.28	1.00	10.67±1.98	13.53±2.02	0.85	10.47±2.18	15.47±2.82	0.57	–	–	–
10.2	2.49±1.11	4.48±1.49	1.00	11.43±1.79	10.52±1.64	0.96	7.05±1.09	7.27±1.01	0.72	–	–	–
10.4	1.99±1.00	1.99±1.00	1.00	8.33±1.43	6.37±1.25	1.00	7.09±0.85	5.37±0.65	0.82	–	–	–
10.6	1.00±0.70	0.50±0.50	1.00	3.74±0.97	4.17±1.01	1.00	3.60±0.47	2.65±0.38	0.90	6.41±1.34	6.47±1.08	0.61
10.8	0.50±0.50	–	1.00	1.32±0.59	1.22±0.55	1.00	1.67±0.30	1.64±0.28	1.00	3.15±0.57	1.84±0.36	0.76
11.0	–	–	–	0.98±0.49	–	1.00	0.67±0.18	0.38±0.13	1.00	1.48±0.28	1.19±0.24	0.86
11.2	–	–	–	–	–	–	0.35±0.13	0.28±0.12	1.00	0.75±0.20	0.81±0.20	0.94
11.4	–	–	–	–	–	–	0.05±0.05	0.05±0.05	1.00	0.45±0.13	0.20±0.09	1.00
11.6	–	–	–	–	–	–	0.05±0.05	–	1.00	0.04±0.04	0.08±0.06	1.00
11.8	–	–	–	–	–	–	–	–	–	0.04±0.04	–	1.00
Tot. Num.	145			166			260			122		

Table 2. Results of STY analysis, and molecular gas mass density. *Top*: results based on Eq. 1. *Bottom*: results obtained with the τ_{dep} scaling of SFR.

Based on Eq. 1	$0.2 < z \leq 0.6$			$0.7 < z \leq 1.0$			$1.0 < z \leq 2.0$			$2.0 < z \leq 3.0$		
	Most prob.	Min.	Max.	Most prob.	Min.	Max.	Most prob.	Min.	Max.	Most prob.	Min.	Max.
Φ^* [$10^{-4} h_{70}^3 \text{Mpc}^{-3} \text{dex}^{-1}$]	11.0	9.8	11.0	7.8	7.4	10.6	5.6	5.3	6.6	–	–	–
$\log(M^*)$ [$h_{70}^{-2} M_{\odot}$]	10.34	10.23	10.34	10.84	10.72	10.86	10.89	10.84	10.94	–	–	–
α	-0.91	-1.08	-0.90	-1.12	-1.15	-1.03	-1.16	-1.16	-1.04	–	–	–
$\rho_{\text{mol}}(\text{tot})$ [$10^7 h_{70} M_{\odot} \text{Mpc}^{-3}$]	2.266	1.751	2.289	5.974	4.317	7.818	4.836	4.112	5.711	–	–	–
$\rho_{\text{mol}}(\text{lim})$ [$10^7 h_{70} M_{\odot} \text{Mpc}^{-3}$]	2.166	1.619	2.188	4.173	3.231	5.361	3.958	3.301	4.972	1.533	1.184	1.882
$\Omega_{\text{mol}}(\text{tot})$ [$10^{-5} h_{70}^{-1}$]	11.34	8.76	11.46	18.00	13.01	23.56	7.19	6.12	8.50	–	–	–
$\Omega_{\text{mol}}(\text{lim})$ [$10^{-5} h_{70}^{-1}$]	10.84	8.10	10.95	12.57	9.74	16.15	5.89	4.91	7.40	0.92	0.71	1.13
Based on τ_{dep}	$0.2 < z \leq 0.6$			$0.7 < z \leq 1.0$			$1.0 < z \leq 2.0$			$2.0 < z \leq 3.0$		
	Most prob.	Min.	Max.	Most prob.	Min.	Max.	Most prob.	Min.	Max.	Most prob.	Min.	Max.
Φ^* [$10^{-4} h_{70}^3 \text{Mpc}^{-3} \text{dex}^{-1}$]	12.0	9.8	13.6	7.4	6.8	9.3	4.9	4.3	6.2	–	–	–
$\log(M^*)$ [$h_{70}^{-2} M_{\odot}$]	10.32	10.27	10.36	10.79	10.70	10.83	10.87	10.83	10.93	–	–	–
α	-1.01	-1.11	-1.00	-1.06	-1.10	-1.00	-1.11	-1.14	-1.04	–	–	–
$\rho_{\text{mol}}(\text{tot})$ [$10^7 h_{70} M_{\odot} \text{Mpc}^{-3}$]	2.540	1.963	3.114	4.725	3.640	6.287	3.880	3.205	5.407	–	–	–
$\rho_{\text{mol}}(\text{lim})$ [$10^7 h_{70} M_{\odot} \text{Mpc}^{-3}$]	2.400	1.810	2.943	3.437	2.771	4.407	3.232	2.590	4.698	1.213	0.929	1.497
$\Omega_{\text{mol}}(\text{tot})$ [$10^{-5} h_{70}^{-1}$]	12.71	9.82	15.59	14.21	10.97	18.94	5.77	4.77	8.04	–	–	–
$\Omega_{\text{mol}}(\text{lim})$ [$10^{-5} h_{70}^{-1}$]	12.01	9.06	14.73	10.36	8.35	13.28	4.81	3.85	6.99	0.73	0.56	0.90

Notes. Minimum and maximum values are computed at the 3σ confidence level. The molecular gas mass density $\rho(\text{tot})$ is obtained by integrating the mass function between $10^7 M_{\odot}$ and infinity; $\rho(\text{lim})$ is computed solely on the mass range covered by PEP data (see Table 1).